

# Dynamic Brazilian Splitting Test of Ring-Shaped Specimens with Different Hole Diameters

Xibing Li<sup>1</sup> · QiuHong Wu<sup>1</sup> · Ming Tao<sup>1</sup> · Lei Weng<sup>1</sup> · Longjun Dong<sup>1</sup> · Yang Zou<sup>2</sup>

Received: 26 January 2016 / Accepted: 20 April 2016 / Published online: 2 May 2016  
© Springer-Verlag Wien 2016

**Keywords** Dynamic loading · Brazilian splitting · Ring-shaped specimen · Full-field strain field · Digital image correlation · Split Hopkinson pressure bar

## 1 Introduction

Defects of unequal scales that exist in natural rocks have a marked effect on the stability and safety of rock mass and are significant in both theoretical and practical applications when studying rock deformation and failure mechanisms (Nemat-Nasser and Horii 1982; Yang et al. 2011). To estimate the influence of defects on the mechanical properties of rock, specimens with pre-existing holes are commonly used in laboratory experiments and numerical simulations (Carter 1992; Tang et al. 2005; Zhao et al. 2010; Li et al. 2015; Lin et al. 2015).

Many researchers use disc-shaped specimens with a pre-drilled hole to study the effect of defects on the development of rock fracturing. Steen et al. (2005) carried out experimental and numerical tests to study the fracture pattern of a loaded disc with an eccentric hole.

You et al. (2011) conducted Brazilian disc tests on both dry and saturated ring-shaped samples with various hole diameters. Wang et al. (2014) studied the failure mechanism of a standard Brazilian disc and discs with a central hole or eccentric hole using a 3D numerical model (RFPA3D). Their results indicate that the peak stress of the specimen decreases as the hole size increases and that the stress around the hole does affect the growth of splitting failure.

However, the aforementioned studies focused mainly on the specimen under static or quasi-static loading conditions, but did not consider dynamic loading, a common occurrence in practical rock engineering. Moreover, the dynamic properties of rock with defects are not fully understood, including the effect of holes on rock deformation and failure mechanisms, and the mechanisms of initiation, propagation, and coalescence of cracks around the hole. Additionally, the applicability of basic assumptions used in split Hopkinson pressure bar (SHPB) tests on ring-shaped specimens needs to be further examined. To clarify the above issues, it is essential to investigate the deformation and failure mechanism of a disc specimen with a hole subjected to dynamic loads.

We present a study of the dynamic mechanical properties of ring-shaped specimens using the dynamic Brazilian test. A modified SHPB apparatus combined with a high-speed (HS) photography system was developed for the study, including a digital image correlation (DIC) technique for measuring the full-field strain fields of the specimens. The stress equilibrium for the ring-shaped specimens in the SHPB system is verified, and the effects of hole size on the peak stress, deformation, and failure mechanisms of the ring-shaped specimen under different loading rates are also investigated in depth.

✉ QiuHong Wu  
0507010223@163.com

<sup>1</sup> School of Resources and Safety Engineering, Central South University, Changsha 410083, Hunan, People's Republic of China

<sup>2</sup> Laboratory of Soil Mechanics, School of Architecture, Civil and Environmental Engineering, École Polytechnique Fédérale de Lausanne (EPFL), Station 18, 1015 Lausanne, Switzerland

## 2 Experimental Method and Preparation

### 2.1 Specimen Preparation

The samples used in this study comprise sandstone obtained from Hengyang, Hunan Province, China. The sandstone was composed of quartz, feldspar, and muscovite and had no macroscopically visible defects in hand specimen. The ring-shaped specimens produced from intact blocks of these samples were 25 mm thick and 50.9 mm in external diameter and had varying hole diameters (0–24 mm).

All the specimens were polished to a roughness of <0.02 mm and were stored in ambient indoor conditions for 7 days. The specimens were labelled after preparation in accordance with their hole diameter and sequence of cutting. For example, “D20-1” indicates that the hole diameter of the specimen is 20 mm and the serial number is 1.

### 2.2 Brazilian Disc Test under Static Load

The Brazilian disc test is a traditional, indirect testing method to obtain the tensile strength of rock based on standards of the International Society for Rock Mechanics (ISRM 1978) and the American Society for Testing and Materials (ASTM 2008). The tensile strength of the disc can be calculated by:

$$T = \frac{2P}{\pi Dt} \quad (1)$$

where  $P$  is the peak force when the specimen fails,  $\pi$  is a circular constant, and  $D$  and  $t$  are the external diameter and thickness of the specimen, respectively.

The above expression of the disc's static tensile strength is normally referred to by the dynamic counterpart tests when the stress equilibrium condition is ensured. According to the Griffith criterion, the Brazilian test is only valid when the primary fracture occurs at the centre of a sound disc (Fairhurst 1964). However, rock does not necessarily behave as a complete brittle material, so the exact central fracturing of the disc may be difficult to ensure. Therefore, ring-shaped specimens have been developed in which a disc with a central hole is subjected to diametric compression, ensuring that the failure initiates at, or near, the hole surface (Hobbs 1965). According to Hobbs (1965), the maximum tensile stress  $T_H$  of a ring test can be determined by:

$$T_H = \frac{2P}{\pi Dt} \left( 6 + 38 \frac{d^2}{D^2} \right) \quad (2)$$

where  $d$  is the hole diameter.

However, the calculated tensile strength for a ring test is much larger than the uniaxial tensile strength when the hole size is very small. The calculated strength tends

asymptotically towards the modulus of rupture (flexural strength) as the hole size increases relative to the outside diameter (Mellor and Hawkes 1971). Therefore, Hobbs' equation, based on elastic mechanics, may not be suitable for determining the tensile strength of the rock.

To evaluate the effect of the hole size on the peak stress of the ring-shaped specimen, You and Su (2010) used the following equation to calculate the peak stress:

$$TT = \frac{2P}{\pi(D-d)t} \quad (3)$$

where  $TT$  is an approximate value of the average tensile stress along the diameter direction (much less than the value of  $T_H$ ) (You 2010). Equation (3) becomes equivalent to Eq. (1) when  $d = 0$ ; to better understand the rationality of Eq. (3), the peak stresses calculated by these equation are described in the following paragraph.

Static Brazilian disc tests were conducted on an Instron (1342) system. Each specimen was placed directly between the loading platens. The contact state of the sample was between the curved loading jaws and flat loading platens with two small-diameter steel rods. The rock samples were loaded under displacement control at a loading rate of 0.002 mm/s. The Brazilian disc tests were conducted three times for each group, and the average value was taken as the peak stress of the specimen.

The peak load of the specimens decreases as the hole diameter decreases, as shown in Table 1. The peak stresses calculated by Eq. (2) are greater than the tensile strengths of the Brazilian disc specimens. This phenomenon has been observed in semicircular bend tests (Dai et al. 2008, 2010b, 2013) in which it was found that determination of rock mechanical parameters should consider the effect of the stress gradient. The peak stresses of the specimens with hole diameter of 8 mm, calculated using Eqs. (3) and (2), are 0.87 and 5.00 times greater than those of the Brazilian disc specimens, respectively. This demonstrates a significant variance from actual test results. Therefore, we proceed with using Eq. (3) in this paper when calculating the stress of ring-shaped specimens.

### 2.3 Dynamic Testing Methods

Dynamic Brazilian splitting experiments were carried out using dynamic loading equipment, as described by Li et al. (2008, 2009, 2011, 2014) (Fig. 1). A semi-sine wave is generated by a special shape striker and used as the loading stress wave. The incident and transmission bars are made of 40Cr alloy steel with a density of 7810 kg/m<sup>3</sup>, Poisson's ratio of 0.28, and Young's modulus of 250 GPa. The P-wave velocities of the bars are 5410 m/s. A HS camera and strain gauges were used to record the whole rock failure process during dynamic loading.

**Table 1** Brazilian fracture results of disc and ring-shaped specimens under static loads

| Specimen no. | Density (kg/m <sup>3</sup> ) | Peak load (N) | $TT$ (MPa) | $T_H$ (MPa) |
|--------------|------------------------------|---------------|------------|-------------|
| D0-1         | 2418                         | 12,047        | 5.80       | 34.79       |
| D0-2         | 2357                         | 11,471        | 5.86       | 35.15       |
| D0-3         | 2417                         | 10,373        | 5.41       | 32.44       |
| Average      |                              |               | 5.69       | 34.12       |
| D8-1         | 2415                         | 8215          | 5.06       | 29.10       |
| D8-2         | 2398                         | 8083          | 4.91       | 28.17       |
| D8-3         | 2409                         | 7810          | 4.88       | 28.01       |
| Average      |                              |               | 4.95       | 28.43       |
| D12-1        | 2413                         | 4683          | 3.13       | 18.93       |
| D12-2        | 2410                         | 4821          | 3.26       | 19.72       |
| D12-3        | 2396                         | 4761          | 3.18       | 19.32       |
| Average      |                              |               | 3.19       | 19.33       |
| D16-3        | 2410                         | 3911          | 2.80       | 18.50       |
| D16-4        | 2385                         | 4370          | 3.10       | 20.35       |
| D16-5        | 2409                         | 3982          | 2.74       | 18.33       |
| Average      |                              |               | 2.88       | 19.06       |
| D20-1        | 2422                         | 2512          | 2.06       | 14.51       |
| D20-2        | 2347                         | 2701          | 2.27       | 16.10       |
| D20-3        | 2417                         | 2621          | 2.14       | 15.38       |
| Average      |                              |               | 2.16       | 15.33       |
| D24-1        | 2473                         | 1735          | 1.70       | 12.54       |
| D24-2        | 2415                         | 1676          | 1.62       | 11.92       |
| D24-3        | 2456                         | 1687          | 1.62       | 11.96       |
| Average      |                              |               | 1.65       | 12.14       |

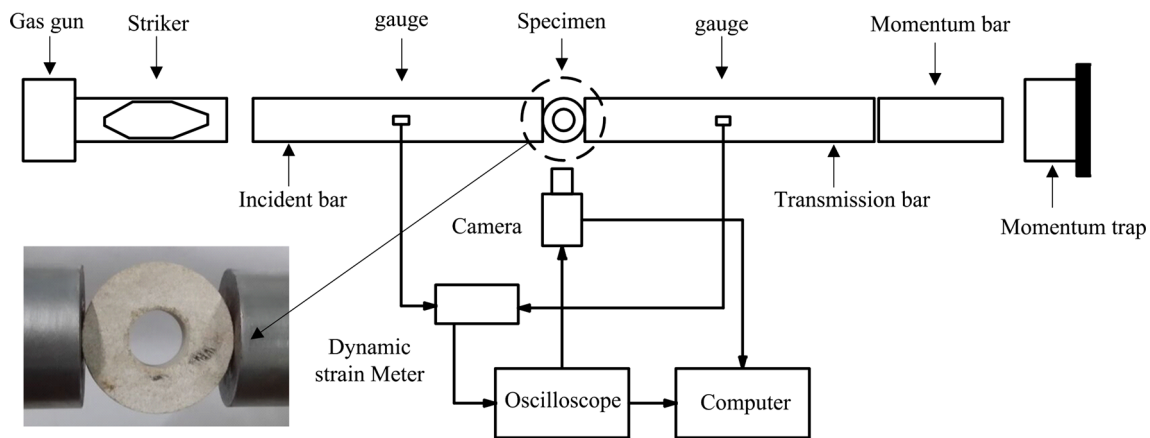


**Fig. 1** Schematic of the split Hopkinson pressure bar system

From one-dimensional stress wave theory, the stresses  $P_1$  and  $P_2$  acting on the ends of the incident bar and transmission bar, respectively, are expressed as:

$$P_1 = AE[\varepsilon_I(t) + \varepsilon_R(t)] \tag{4}$$

$$P_2 = AE\varepsilon_T(t) \tag{5}$$

where  $E$  is the Young's modulus of the pressure bars,  $A$  is the cross-sectional area of the bars, and  $\varepsilon_I(t)$ ,  $\varepsilon_R(t)$ , and

$\varepsilon_T(t)$  are the strain signals of the incident wave, reflected wave, and transmitted wave, respectively.

The average loading pressure on the specimens is shown in Eq. (6), and provided the specimen is in a state of stress equilibrium, the inertial effect can be ignored, as shown in Eq. (7):

$$P(t) = (P_1 + P_2)/2 = AE[\varepsilon_I(t) + \varepsilon_R(t) + \varepsilon_T(t)]/2 \tag{6}$$

$$\varepsilon_I(t) + \varepsilon_R(t) = \varepsilon_T(t) \quad (7)$$

Finally, substituting Eq. (7) into Eq. (6) gives:

$$P(t) = AE\varepsilon_T(t) \quad (8)$$

Under the conditions of stress equilibrium during dynamic loading, the dynamic strength can be calculated by substituting Eq. (8) into Eq. (3).

### 3 Experimental Results

#### 3.1 Stress Equilibrium

In dynamic experiments, the stresses acting on the two ends of the specimen are different, resulting in an imbalanced loading state; hence, the inertial effect cannot be ignored. To diminish the inertial effect, the specimen must reach a state of stress equilibrium before the rock fails. It is a prerequisite for the reliability of the experimental results.

Figure 2a shows the incident and reflected stresses recorded in the dynamic loading experiment at the ends of a specimen with a hole diameter of 24 mm. Though a very small transmitted stress wave was generated, the sum of the incident stress and reflected stress was markedly different from the transmitted stress during the whole loading process. This indicates that the stresses at the two ends of the specimen were unequal, and therefore, the peak stress analysis of this specimen was exclusive.

The stress wave signals of specimen D20-10 from the dynamic loading experiment are shown in Fig. 2b. The failure of the specimen can be assessed from the peak stress at 60  $\mu\text{s}$ . After that time, the transmitted stress decreases gradually, but the deviation of the stresses at the two ends of the specimen increases, indicating a state of disequilibrium and thus damage to the specimen. Nevertheless, before the stress peak point, the transmitted wave was very close to the sum of the incident wave and reflected wave, indicating that the specimen reached and maintained a state of stress equilibrium before failure.

To further validate the stress equilibrium state of the specimen, strain gauges of  $5 \times 3$  mm in size were used to record the strains at several special locations on the specimen. Four strain gauges were glued to the circular surface of specimen D16-6. Gauges 2 and 4 were located around the periphery of the hole, while gauges 5 and 6 were placed 20 mm from the specimen centre (Fig. 3). The damage at the four monitored locations occurred at 446, 444, 461, and 458  $\mu\text{s}$ , respectively, illustrating that the cracks were initiated simultaneously at the two hole regions where tensile stress was induced. It also shows that the specimen was fractured after reaching a state of stress equilibrium. Therefore, it is considered that the reliability of the

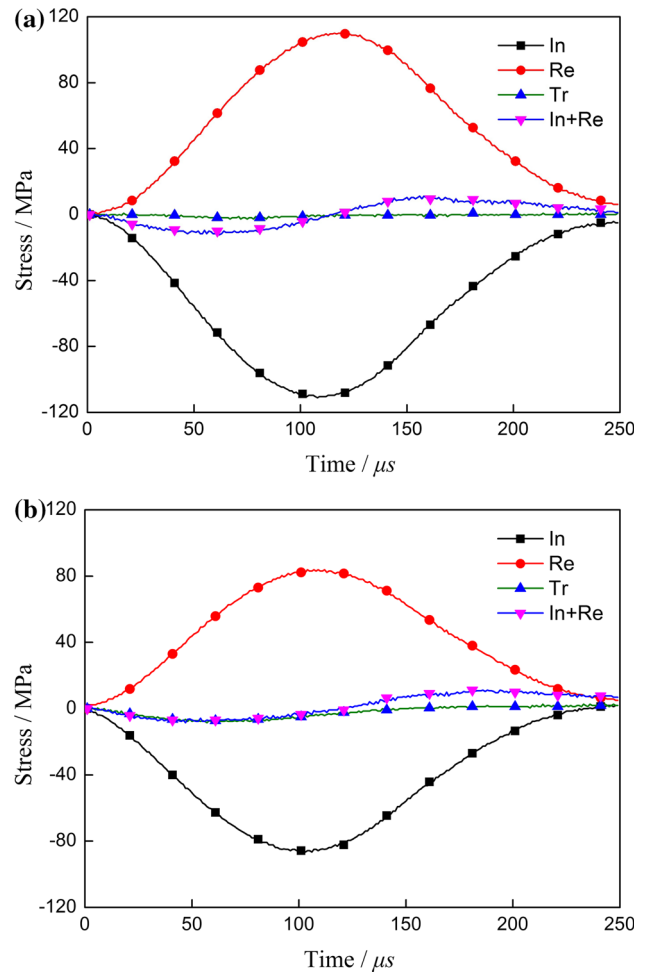


**Fig. 2** Dynamic stress on both ends of the ring-shaped specimens tested using a modified SHPB, **a** D24-4, **b** D20-10

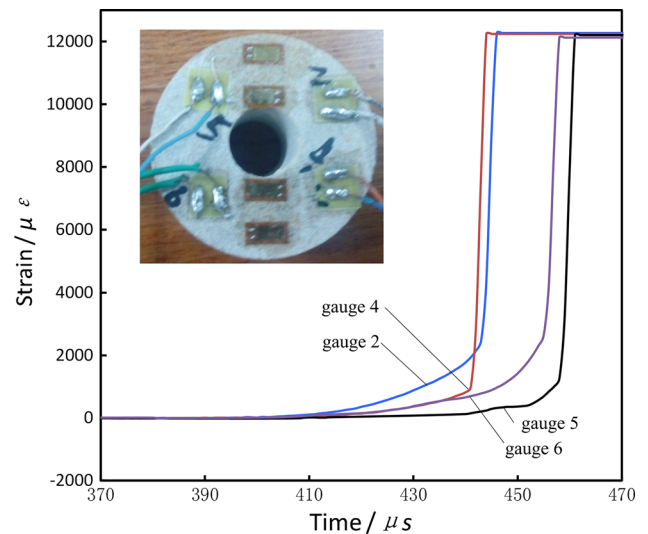


**Fig. 3** Deformation information of specimen D16-6 obtained by strain gauges on its surface

experimental results is verifiable and the peak stress value obtained is valid.

### 3.2 Dynamic Peak Stress

The mechanical parameters of the specimens subjected to dynamic loading are shown in Table 2. The loading rate is defined as the slope of the approximate linear phase in a

stress–time curve (Dai et al. 2010a). The dynamic peak stress of the sandstone specimens under various loading rates is plotted in Fig. 4, wherein it is evident that the dynamic peak stress for each specimen is greater than the static peak stress.

Despite severe stress concentration appearing on the surface of the hole along the loading direction, the static and dynamic bearing capacity of the ring-shaped specimen with an 8-mm-diameter hole is close to that of the Brazilian disc

**Table 2** Mechanical parameters under dynamic loads

| Specimen no. | Density (kg/m <sup>3</sup> ) | Hole diameter (mm) | Loading rate (GPa/s) | Dynamic peak stress (MPa) |
|--------------|------------------------------|--------------------|----------------------|---------------------------|
| D0-4         | 2408                         | 0                  | 394.7                | 16.88                     |
| D0-5         | 2423                         | 0                  | 592.9                | 20.00                     |
| D0-6         | 2460                         | 0                  | 510.5                | 21.49                     |
| D0-7         | 2377                         | 0                  | 423.8                | 22.14                     |
| D0-8         | 2428                         | 0                  | 317.1                | 18.65                     |
| D0-9         | 2432                         | 0                  | 493.8                | 20.91                     |
| D0-10        | 2410                         | 0                  | 187.5                | 17.26                     |
| D8-4         | 2397                         | 8                  | 400.8                | 17.33                     |
| D8-5         | 2393                         | 8                  | 379.1                | 19.03                     |
| D8-6         | 2401                         | 8                  | 295.5                | 16.55                     |
| D8-7         | 2382                         | 8                  | 329.9                | 17.16                     |
| D8-8         | 2403                         | 8                  | 560.9                | 18.93                     |
| D8-9         | 2397                         | 8                  | 433.9                | 18.21                     |
| D8-10        | 2384                         | 8                  | 170.3                | 14.14                     |
| D8-11        | 2415                         | 8                  | 124.6                | 13.58                     |
| D8-12        | 2377                         | 8                  | 233.4                | 14.94                     |
| D8-13        | 2429                         | 8                  | 482.4                | 18.07                     |
| D12-4        | 2329                         | 12                 | 194.8                | 11.88                     |
| D12-5        | 2553                         | 12                 | 180.1                | 10.80                     |
| D12-6        | 2292                         | 12                 | 242.5                | 11.88                     |
| D12-7        | 2382                         | 12                 | 315.9                | 13.53                     |
| D12-8        | 2345                         | 12                 | 408.7                | 14.74                     |
| D12-9        | 2335                         | 12                 | 574.1                | 15.55                     |
| D16-4        | 2358                         | 16                 | 315.2                | 14.03                     |
| D16-5        | 2389                         | 16                 | 102.3                | 7.98                      |
| D16-6        | 2434                         | 16                 | 210.6                | 8.71                      |
| D16-7        | 2412                         | 16                 | 639.1                | 15.80                     |
| D16-8        | 2441                         | 16                 | 302.6                | 12.61                     |
| D16-9        | 2412                         | 16                 | 339.3                | 14.25                     |
| D16-10       | 2393                         | 16                 | 441.2                | 11.67                     |
| D16-11       | 2425                         | 16                 | 666.6                | 16.11                     |
| D20-4        | 2483                         | 20                 | 143.8                | 6.61                      |
| D20-5        | 2486                         | 20                 | 247.6                | 8.42                      |
| D20-6        | 2391                         | 20                 | 122.7                | 6.01                      |
| D20-7        | 2478                         | 20                 | 167.1                | 6.52                      |
| D20-8        | 2428                         | 20                 | 357.5                | 9.18                      |
| D20-9        | 2389                         | 20                 | 507.5                | 10.37                     |
| D20-10       | 2426                         | 20                 | 607.9                | 11.87                     |
| D20-11       | 2388                         | 20                 | 552.4                | 9.99                      |

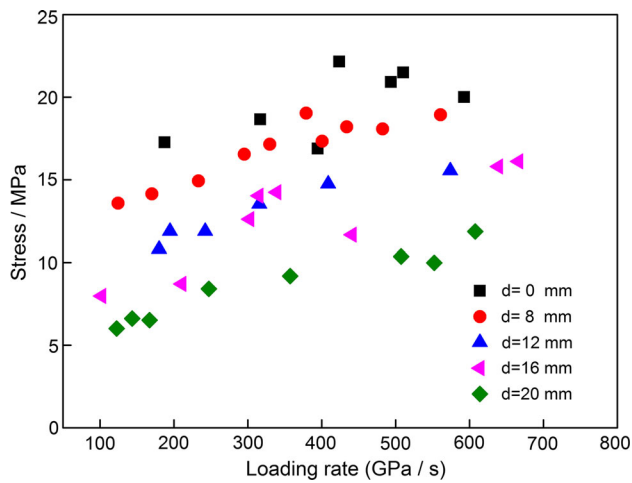


**Fig. 4** The dynamic peak stress of the specimens under different loading rates

specimen, suggesting that a small-diameter hole has little influence on the peak stress of the ring-shaped specimen.

The distance between the hole surface and the loading end decreases as the hole diameter increases, reducing the stresses of the loading ends along the loading direction. When the diameter is  $>16$  mm, the strength of the ring-shaped specimen decreases considerably; thus, the larger the hole diameter, the greater the influence on the dynamic peak stress of the ring-shaped specimen.

### 3.3 Deformation Characteristics

By employing traditional contact measurement methods, such as the electromotive strain testing method and acoustic emission monitoring, the rock failure process can be effectively observed during the experiments. These experimental techniques are quite simple and convenient, but it is difficult to obtain a comprehensive data set of the whole rock failure process. A non-contact optical measurement method known as the digital image correlation (DIC) technique has been widely used to measure deformation in experimental mechanics (Hild and Roux 2006; Pan 2011; Reu and Miller 2008). The DIC technique is advantageous, because it has relatively low demands in terms of light source, from specimen set-up, or from the overall experimental environment. By using DIC and HS camera techniques, the dynamic failure process of a rock specimen can be observed under various loading rates. The DIC technique has been successfully applied in recent rock material tests (Song et al. 2013; Nguyen et al. 2011; Ma et al. 2004; Zhang and Zhao 2013) and Chen et al. (2014) specifically investigated the dynamic tensile strength of three brittle materials and analysed the dynamic deformation and failure modes using DIC. In this study, the full-

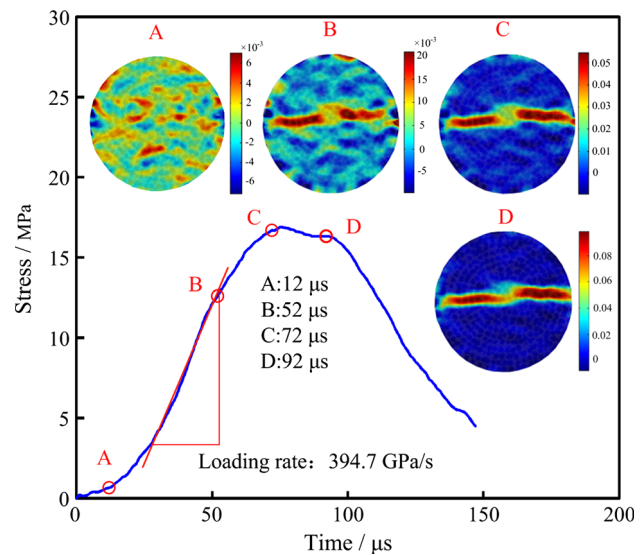


**Fig. 5** The evolution of vertical strain fields of specimen D0-4 under dynamic loads

field deformation characteristics of ring-shaped sandstone specimens with different hole diameters are examined using the SHPB system with a semi-sine wave.

In our experiment, the HS camera was triggered by a transistor–transistor-logic pulse that was determined from the incident wave, thus achieving synchronization of the HS camera and oscilloscope. The resolution of the image is  $384 \times 256$  pixels, captured at a frame rate of 50,000 fps. Considering the quality of the speckle pattern (Yu et al. 2014) and the deformation status of the rock specimen, a small sub-zone of the image ( $21 \times 21$  pixels) was chosen for point-by-point calculation. Note that the specimen loading direction was horizontal and the stress wave originated from the right bar.

The evolution of the vertical strain fields of specimen D0-4 is shown in Fig. 5. The calculation region contains the whole circular area which has a 50 mm diameter. The incident and transmission bars are in close contact with the sample in the initial loading stage, and the specimen ends have no obvious areas of strain concentration. As the load increases, a zone of tensile strain concentration appears near the centre of the Brazilian disc along the loading direction. The tensile strain values near the centre of the disc are much greater than at the loading ends of the sample. The tensile strain in this concentrated zone gradually increases with longer loading times and extends towards the loading ends along the loading direction, finally coalescing across the specimen. The HS camera images show that the crack initiates near the centre of the disc in agreement with results of strain gauge measurements (Zhou et al. 2013).

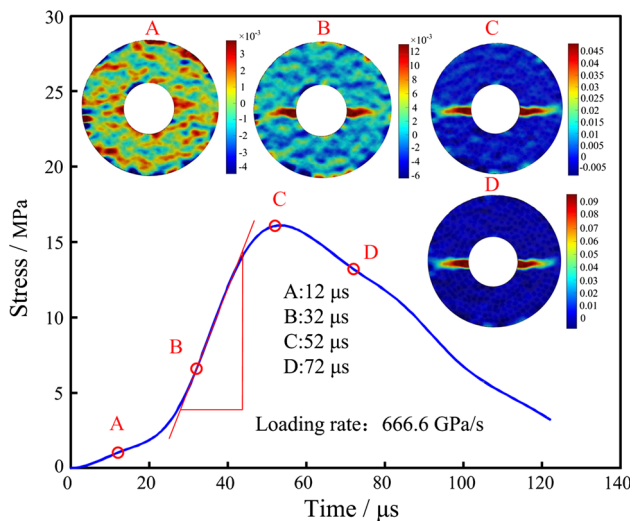


**Fig. 6** The evolution of vertical strain fields of specimen D16-11 under dynamic loads

There is little difference between the failure modes of the various ring-shaped specimens, so we only present the analysis of specimen D16-11. The evolution of the vertical strain fields of specimen D16-11 is shown in Fig. 6. The DIC calculated area is the ring-shaped area with an external diameter of 50 mm and hole diameter of 16 mm.

In the initial stage (stage A), different levels of damage were observed on the specimen surface, and the regions around the hole along the loading direction have relatively high concentrations of stress. Under continued loading, the symmetry of the tensile strain zones around the hole along the loading direction is evident (stage B), indicating that stress equilibrium can occur at this stage. In the final stages, the tensile strain zone extends towards the two loading ends until the specimen fails. The evolution of the full-field strain shows that the DIC technique is a convenient method to fully capture and interpret the dynamic failure process, especially for specimens that deform non-uniformly in time and discontinuously in space.

### 3.4 Failure Patterns of Specimens

Under static loading, most of the specimens split into two complete fragments, with the fracture plane parallel to the loading direction (Fig. 7a). One ring-shaped specimen with a 16-mm hole splits into four fragments under static loading conditions. Under dynamic loading (Fig. 7b), wedge-shaped crushed zones were induced near the loading ends of the disc specimen. This is because of secondary fractures that follow the primary fractures from the centre of the disc. This result is similar to the results of previous work conducted in dynamic testing (Zhu and Tang 2006;

Dai et al. 2010a; Zhou et al. 2014; Wu et al. 2015). With an increased loading rate, the angle of the crushed zone increases. The crushed zone develops after the primary fracture forms near the centre, and so it does not influence the validity of the experimental results.

In Fig. 7b the dynamic loading rates of the first five samples are, in GPa/s, 493.8, 170.3, 242.5, 339.3, and 357.5, respectively. The loading rate for sample D8-10 is relatively low, and the failure mode is similar to that of the intact disc sample. The specimens with larger holes fractured into four parts (Fig. 7b). You et al. (2011) conducted static loading experiments on ring-shaped specimens using two loading methods, i.e. flattened loading with two small-diameter steel rods and direct flattened loading. The results showed that the specimen fractured into two parts when loaded by steel rods, but fragmented into four parts when using direct flattened loading. Thus, the fracture mode of the ring-shaped specimen is closely associated with the loading method, and explains why four fragments of the ring-shaped specimen were generated during dynamic impact by flattened loading in our experiments. The ring-shaped specimen fractured into four pieces because the incident bar continued to apply force to the semi-ring structures, causing the specimen to break into four pieces.

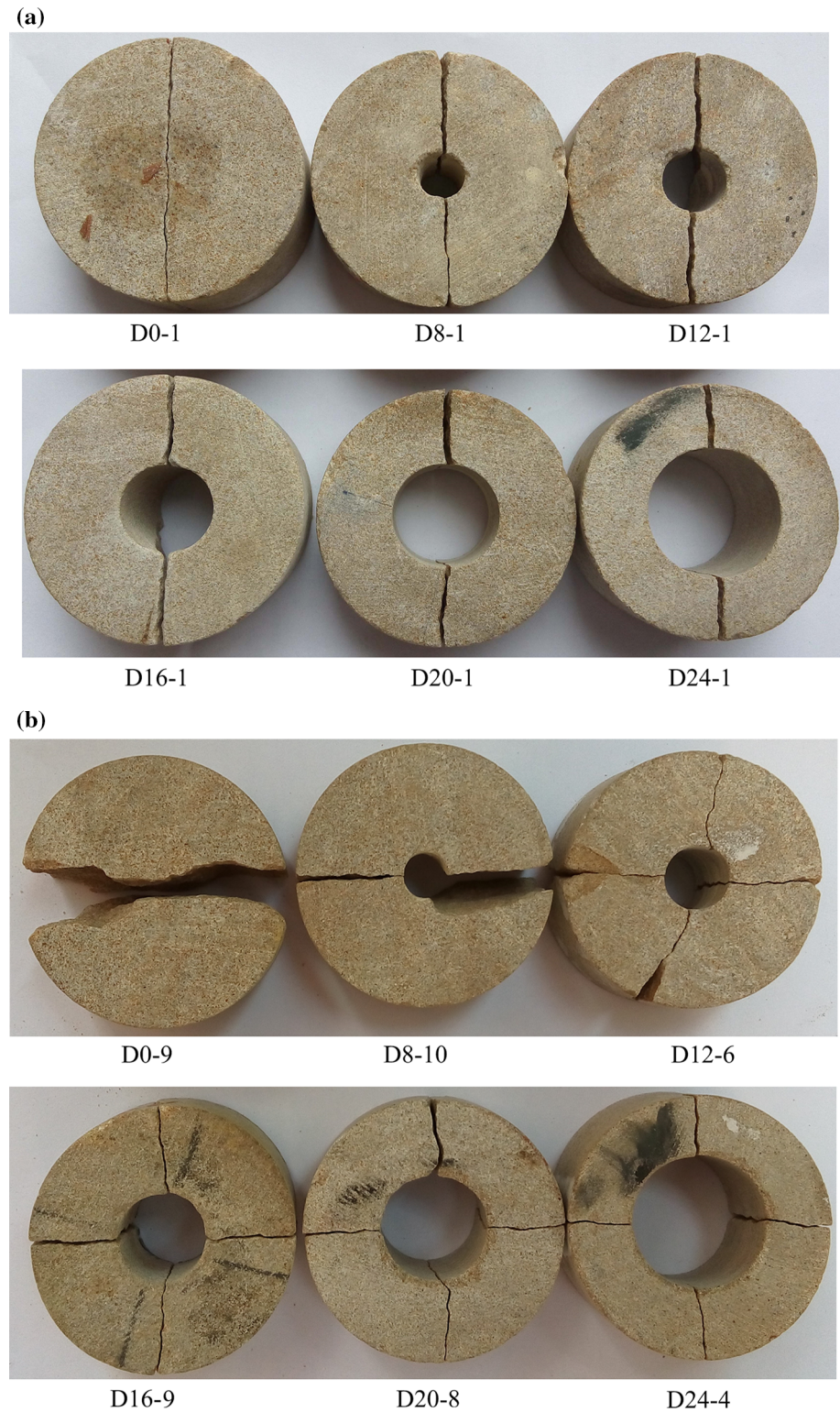
One of the significant findings of this investigation is that the size of the crushed zone of the ring-shaped specimen is smaller than that of the disc specimen, and the wedge-shaped crushed zone is similar in size. This is because the stress is concentrated around the hole along the loading direction; hence, the initial crack occurs away from the loading ends.

## 4 Conclusions

The dynamic Brazilian splitting test was used to study the effect of specimen hole diameter on the dynamic peak stress, deformation characteristics, and failure mechanisms of rock specimens. A modified SHPB system was used to apply dynamic loading and digital image correlation (DIC) was used to investigate the deformation behaviour of the loaded specimens using images recorded by a HS camera.

Several conclusions can be drawn from this study: (1) the basic assumptions related to SHPB testing of ring-shaped specimens are verified; (2) dynamic peak stress decreases with increasing hole diameter; (3) the surface full-field deformation results recorded by DIC during dynamic loading can be considered reliable; and (4) most of the ring-shaped specimens split into two fragments under static loads, or four parts under dynamic loading.

**Fig. 7** Typical failure patterns of specimens under static and dynamic loads, **a** static loads in vertical direction, **b** dynamic loads in horizontal direction



Additionally, the size of the crushed zone of the ring-shaped specimens is smaller than that of the disc specimens, resulting from stress concentration around the hole.

**Acknowledgments** This paper was supported by the National Natural Science Foundation of China (41272304, 11472311) and Hunan Provincial Innovation Foundation for Postgraduate (71380100005).

## References

- ASTM (2008) D 3967-08: standard test method for splitting tensile strength of intact rock core specimens. ASTM International, West Conshohocken
- Carter BJ (1992) Size and stress gradient effects on fracture around cavities. *Rock Mech Rock Eng* 25:167–186
- Chen JJ, Guo BQ, Liu HB, Liu H, Chen PW (2014) Dynamic Brazilian test of brittle materials using the split Hopkinson pressure bar and digital image correlation. *Strain* 50(6):563–570
- Dai F, Xia K, Luo SN (2008) Semicircular bend testing with split Hopkinson pressure bar for measuring dynamic tensile strength of brittle solids. *Rev Sci Instrum* 79(12):123903–123906
- Dai F, Huang S, Xia KW, Tan ZY (2010a) Some fundamental issues in dynamic compression and tension tests of rocks using split Hopkinson pressure bar. *Rock Mech Rock Eng* 43(6):657–666
- Dai F, Xia K, Tang L (2010b) Rate dependence of the flexural tensile strength of laurentian granite. *J Rock Mech Min Sci* 47(3):469–475
- Dai F, Xia K, Zuo JP, Zhang R, Xu NW (2013) Static and dynamic flexural strength anisotropy of barre granite. *Rock Mech Rock Eng* 46(6):1589–1602
- Fairhurst C (1964) On the validity of the ‘Brazilian’ test for brittle material. In *J Rock Mech Min Sci* 1:535–564
- Hild F, Roux S (2006) Digital image correlation: from displacement measurement to identification of elastic properties: a review. *Strain* 242:69–80
- Hobbs DW (1965) An assessment of a technique for determining the tensile strength of rock. *Br J Appl Phys* 16(2):259–268
- ISRM (1978) Suggested methods for determining tensile strength of rock materials. *Int J Rock Mech Min Sci Abstr* 15(3):99–103
- Li XB, Zhou ZL, Lok TS, Hong L, Yin TB (2008) Innovative testing technique of rock subjected to coupled static and dynamic loads. *Int J Rock Mech Min Sci* 45(5):739–748
- Li XB, Zhou ZL, Hong L, Yin TB (2009) Large diameter SHPB tests with a special shaped striker. *ISRM News J* 12:76–79
- Li XB, Zhou ZL, Liu DS, Zou Y, Yin TB (2011) Wave shaping by special shaped striker in SHPB tests. In: Zhou Y, Zhao J (eds) *Advances in rock dynamics and applications*. CRC Press, Taylor & Francis Group, Boca Raton, pp 105–124
- Li XB, Zou Y, Zilong Zhou (2014) Numerical simulation of the rock SHPB test with a special shape striker based on the discrete element method. *Rock Mech Rock Eng* 47(5):1693–1709
- Li DY, Cheng TJ, Zhou T, Li XB (2015) Experimental study of the dynamic strength and fracturing characteristics of marble specimens with a single hole under impact loading. *Chin J Rock Mech Eng* 34(2):449–460 (in Chinese)
- Lin P, Wong RHC, Tang CA (2015) Experimental study of coalescence mechanisms and failure under uniaxial compression of granite containing multiple holes. *Int J Rock Mech Min Sci* 77:313–327
- Ma SP, Xu XH, Zhao YH (2004) The GEO-DSCM system and its application to the deformation measurement of rock materials. *Int J Rock Mech Min Sci* 41:292–297
- Mellor M, Hawkes I (1971) Measurement of tensile strength by diametral compression of discs and annuli. *Eng Geol* 5(3):173–225
- Nemat-Nasser S, Horii H (1982) Compression-induced nonlinear crack extension with application to splitting, exfoliation, and rockburst. *J Geophys Res* 87(B8):6805–6821
- Nguyen TL, Hall SA, Vacher P, Viggiani G (2011) Fracture mechanisms in soft rock: identification and quantification of evolving displacement discontinuities by extended digital image correlation. *Tectonophysics* 503:117–128
- Pan B (2011) Recent progress in digital image correlation. *Exp Mech* 51(7):1223–1235
- Reu PL, Miller TJ (2008) The application of high-speed digital image correlation. *J Strain Anal Eng Des* 43:673–688
- Song HP, Zhang H, Kang YL, Huang GY, Fu DG, Qu CY (2013) Damage evolution study of sandstone by cyclic uniaxial test and digital image correlation. *Tectonophysics* 608:1343–1348
- Steen BVD, Vervoort A, Napier JAL (2005) Observed and simulated fracture pattern in diametrically loaded discs of rock material. *Int J Fract* 131(1):35–52
- Tang CA, Wong RHC, Chau KT, Lin P (2005) Modeling of compression-induced splitting failure in heterogeneous brittle porous solids. *Eng Fract Mech* 72(4):597–615
- Wang SY, Sloan SW, Tang CA (2014) Three-dimensional numerical investigations of the failure mechanism of a rock disc with a central or eccentric hole. *Rock Mech Rock Eng* 47(6):2117–2137
- Wu BB, Chen R, Xia KW (2015) Dynamic tensile failure of rocks under static pre-tension. *Int J Rock Mech Min Sci* 80:12–18
- Yang SQ, Yang DS, Jing HW, Li YH, Wang SY (2011) An experimental study of the fracture coalescence behaviour of brittle sandstone specimens containing three fissures. *Rock Mech Rock Eng* 45(4):563–582
- You M (2010) Strength and failure of rock due to hydraulic fracture. In: Xie F (ed) *Rock stress and earthquakes*. Taylor & Francis, London, pp 185–188
- You MQ, Su CD (2010) Study on strength and failure of hollow cylinders and rings of sandstone under compression-tension stresses. *Chin J Rock Mech Eng* 29(6):1096–1105 (in Chinese)
- You MQ, Chen XL, Su CD (2011) Brazilian splitting strengths of discs and rings of rocks in dry and saturated conditions. *Chin J Rock Mech Eng* 30(3):464–472 (in Chinese)
- Yu H, Guo R, Xia H, Yan F, Zhang Y, He T (2014) Application of the mean intensity of the second derivative in evaluating the speckle patterns in digital image correlation. *Opt Laser Eng* 60(5):32–37
- Zhang QB, Zhao J (2013) Determination of mechanical properties and full-field strain measurements of rock material under dynamic loads. *Int J Rock Mech Min Sci* 60:423–439
- Zhao C, Matsuda H, Morita C, Shen MR (2010) Study on failure characteristic of rock-like materials with an open-hole under uniaxial compression. *Strain* 47(5):405–413
- Zhou ZL, Zou Y, Li XB, Jiang YH (2013) Stress evolution and failure process of Brazilian disc under impact. *J Central South Univ Technol* 20(1):172–177
- Zhou ZL, Li XB, Zou Y, Jiang YH, Li GH (2014) Dynamic Brazilian tests of granite under coupled static and dynamic loads. *Rock Mech Rock Eng* 47(2):495–505
- Zhu WC, Tang CA (2006) Numerical simulation of Brazilian disk rock failure under static and dynamic loading. *Int J Rock Mech Min Sci* 43(2):236–252